Deep-Sea Research I 56 (2009) 1–14

Contents lists available at ScienceDirect

Deep-Sea Research I

journal homepage: www.elsevier.com/locate/dsri

Seasonal variability in Atlantic Water off Spitsbergen

Vladimir V. Ivanov [a,*], Igor V. Polyakov [a], Igor A. Dmitrenko [b], Edmond Hansen [c], Irina A. Repina [d], Sergey A. Kirillov [e], Cecillie Mauritzen [f], Harper Simmons [a], Leonid A. Timokhov [e]

[a] International Arctic Research Center (IARC), University of Alaska (UAF), 930 Koyukuk Drive, PO Box 757335, Fairbanks, AK 99775-7335, USA
[b] Leibniz Institute of Marine Sciences, University of Kiel, Kiel, Germany
[c] Norwegian Polar Institute, Tromso, Norway
[d] Obukhov Institute of Atmospheric Physics, Moscow, Russian Federation
[e] Arctic and Antarctic Research Institute, St. Petersburg, Russian Federation
[f] Norwegian Meteorological Institute, Oslo, Norway

ARTICLE INFO

Article history:
Received 26 July 2007
Received in revised form
23 July 2008
Accepted 29 July 2008
Available online 8 August 2008

Keywords:
Seasonal variations
Time series
Statistical analysis
Arctic Ocean
Atlantic Water

ABSTRACT

A combination of 2-year-long mooring-based measurements and snapshot conductivity–temperature–depth (CTD) observations at the continental slope off Spitsbergen (81°30′N, 31°00′E) is used to demonstrate a significant hydrographic seasonal signal in Atlantic Water (AW) that propagates along the Eurasian continental slope in the Arctic Ocean. At the mooring position this seasonal signal dominates, contributing up to 50% of the total variance. Annual temperature maximum in the upper ocean (above 215 m) is reached in mid-November, when the ocean in the area is normally covered by ice. Distinct division into 'summer' (warmer and saltier) and 'winter' (colder and fresher) AW types is revealed there. Estimated temperature difference between the 'summer' and 'winter' waters is 1.2 °C, which implies that the range of seasonal heat content variations is of the same order of magnitude as the mean local AW heat content, suggesting an important role of seasonal changes in the intensity of the upward heat flux from AW. Although the current meter observations are only 1-year long, they hint at a persistent, highly barotropic current with little or no seasonal signal attached.

Published by Elsevier Ltd.

1. Introduction

It is well established that the Arctic ice cover and the near surface water layer are subject to large seasonal variations (e.g. Polyakov et al., 1999). However, very little is known about how deeply these variations penetrate into the water column. It is generally assumed that over most of the Arctic Ocean the depth at which the regular seasonal signal can be distinguished is limited by the depth of the permanent thermocline/halocline (e.g. Rudels et al., 1996). This depth depends on the region and varies from ~50–100 m in the Eurasian Basin to ~30–40 m in the Canadian Basin (EWG, 1997, 1998; Rudels et al., 2004). The seasonal signal may also be translated from sub-Arctic seas with Atlantic and Pacific inflows. This fact is well documented for Pacific water inflow through the Bering Strait (Nikiforov and Shpaikher, 1980). Summer (warmer and fresher) and winter (colder and saltier) Pacific-origin waters propagate over long distances in the Arctic Ocean, keeping their distinctive temperature and salinity properties (Steele et al., 2004). For Atlantic Water (AW) inflow through Fram Strait a similar division has not been documented, although the existence of a strong seasonal signal in water temperature in the West Spitsbergen Current is confirmed by multiyear measurements in Fram Strait (Schauer et al., 2004).

In this study, we analyze a set of 2-year-long time series of temperature and salinity data and 1-year-long time series of current velocity data in the pathway of AW inflow northeast of Spitsbergen. Our main purpose in

* Corresponding author. Tel.: +19074742678; fax: +19074742643.
E-mail address: vivanov@iarc.uaf.edu (V.V. Ivanov).

0967-0637/$ - see front matter Published by Elsevier Ltd.
doi:10.1016/j.dsr.2008.07.013

making these measurements was to examine the boundary current over the slope in the area where it 'leaves' the surface and transforms into an intermediate water flow. Collected time series demonstrate that a strong and persistent seasonal cycle dominates the variability of water properties deep in the water column. This finding provided the major focus of this paper. Specific objectives include (i) relating mooring-based observations to background thermohaline and dynamical conditions; (ii) estimating the relative significance of seasonal signal among the other variability modes resolved by the time series; (iii) estimating seasonal cycle parameters (amplitude and phase), and (iv) quantifying seasonal changes in water properties.

2. Data description

In September 2004, scientists from the Norwegian Polar Institute (NPI, Norway) and the International Arctic Research Center (IARC, USA) jointly deployed a mooring in 1010 m of water at 81°30′N, 31°00′E from R/V *Lance* and carried out an oceanographic cross-section in the vicinity of Spitsbergen (Fig. 1). The mooring was equipped with five SBE37 conductivity–temperature–depth (CTD) meters deployed at 70, 112, 215, 465, and 992 m, and three RCM-9 current meters deployed at 69, 216, and 993 m (see schematic representation in Fig. 1), because of severe ice conditions this mooring was not retrieved as planned in 2005. In September 2006 the mooring was successfully recovered and the CTD cross-section was repeated. All instruments worked until the batteries died and provided continuous records. The longest current record is a little over a year in duration, and all temperature/conductivity records cover a complete 2-year time span. The SBE37s took measurements every 15 min. Current velocity was registered once every hour. After-cruise calibration showed a relatively large, strongly negative salinity trend (−0.0012 1/month) at the SBE37 deployed at 465 m. Calibration tests showed that all other instruments performed in satisfactorily. However, although the SBE37 deployed at 992 m passed its calibration test, its salinity record also showed a strong negative salinity trend that is not confirmed by the temperature record taken by the same instrument or by accompanying CTD profiles. Therefore, salinity records from the two deepest instruments were considered unreliable and were not used. Accuracies of individual temperature and conductivity measurements are ±0.002 °C and ±0.0003 S/m, respectively; accuracies of current velocity and direction measurements are ±1% of reading and ±7.5°, respectively. Mooring-based observations were complemented by CTD snapshot measurements (surveys) carried out from R/V *Lance* in 2004 and from the icebreaker *Kapitan Dranitsyn* in 2006. A shipboard Seabird SBE911plus CTD profiler was employed on *Lance*, and an SBE19 on *Kapitan Dranitsyn*. Accuracies of individual temperature and conductivity measurements are ±0.005 °C and ±0.0005 S/m, respectively. CTD sensors successfully passed after-cruise calibration. In this study we used linearly interpolated CTD data with a 1 m vertical increment. Raw data processing included a sequence of routine procedures designed to eliminate erroneous data. These procedures are described in the Appendix A.

3. Data analysis

3.1. Cross-slope thermohaline structure at the mooring position in summer

A cross-slope section around 30°E was sampled earlier, in July 1991 (Schauer, 1995) and in August 1993 (Schauer et al., 1997). Vertical distributions of temperature and

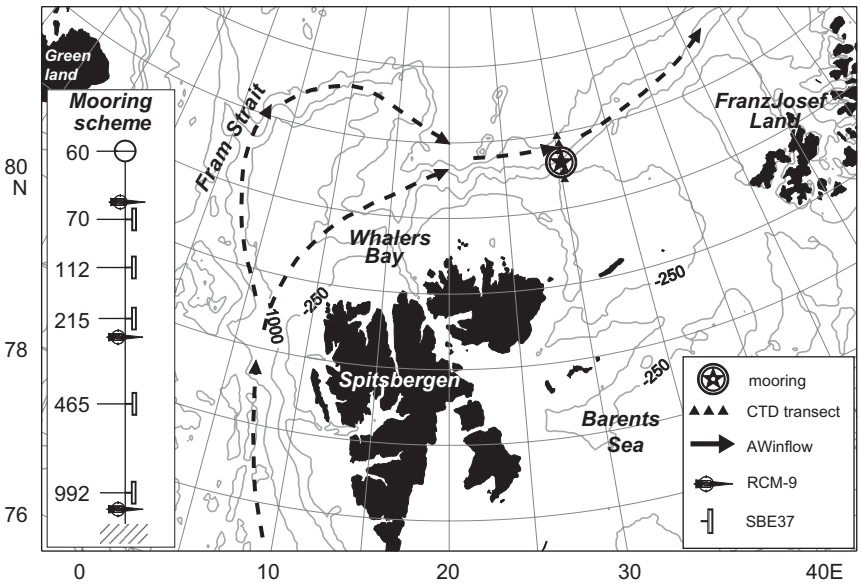

Fig. 1. Location of the mooring and CTD transect, topography in the Arctic Ocean, and Atlantic Water inflow. Mooring schematics are shown in the left inset. Symbols are explained in the right inset.

salinity in September 2004 and 2006 (Fig. 2) demonstrate features similar to those described in the referenced papers. The subsurface temperature maximum indicates the core of AW flow. The depth of this maximum varies from year to year, ranging from 200 m in 1993 to 50 m in 2006. There is large inter-annual variability of maximum temperature, from 2.9 °C in July 1991 to 5.6 °C in September 2006. Spatial location of the AW core (defined by the maximum temperature) is remarkably stable relative to the bottom topography. The salinity maximum generally occurs at the same station, but somewhat deeper than the temperature maximum. In 1991, 1993, and 2004 the AW core was found within the 5-mile range that exists between the 700 and 1000 m isobaths. The 2006 survey was the only case when maximum temperature was observed closer to the shelf. However, as follows from Fig. 2, this did not occur because the warm core as a whole had shifted shoreward, but rather because it had expanded horizontally and split into two parts. The shallow warm and salty core formed over the 500 m isobath, while the deep core kept the same position as in earlier years. In contrast with surveys conducted in the 1990s, when the upper 50 m layer was occupied by water of negative temperature, during both of our surveys positive temperature water reached the surface. The upper ocean salinity was less than 34.0. The lower boundary of AW (zero-degree isotherm) during both surveys was located between 800 and 900 m. The mooring was deployed in the AW core, as seen in the cross-slope section from September 2004 (Fig. 2a).

3.2. Mean vertical thermohaline and dynamical structure at the mooring position

In this section we relate temperature, salinity, and currents, temporally averaged over the period of measurements, with other available pieces of information: climate

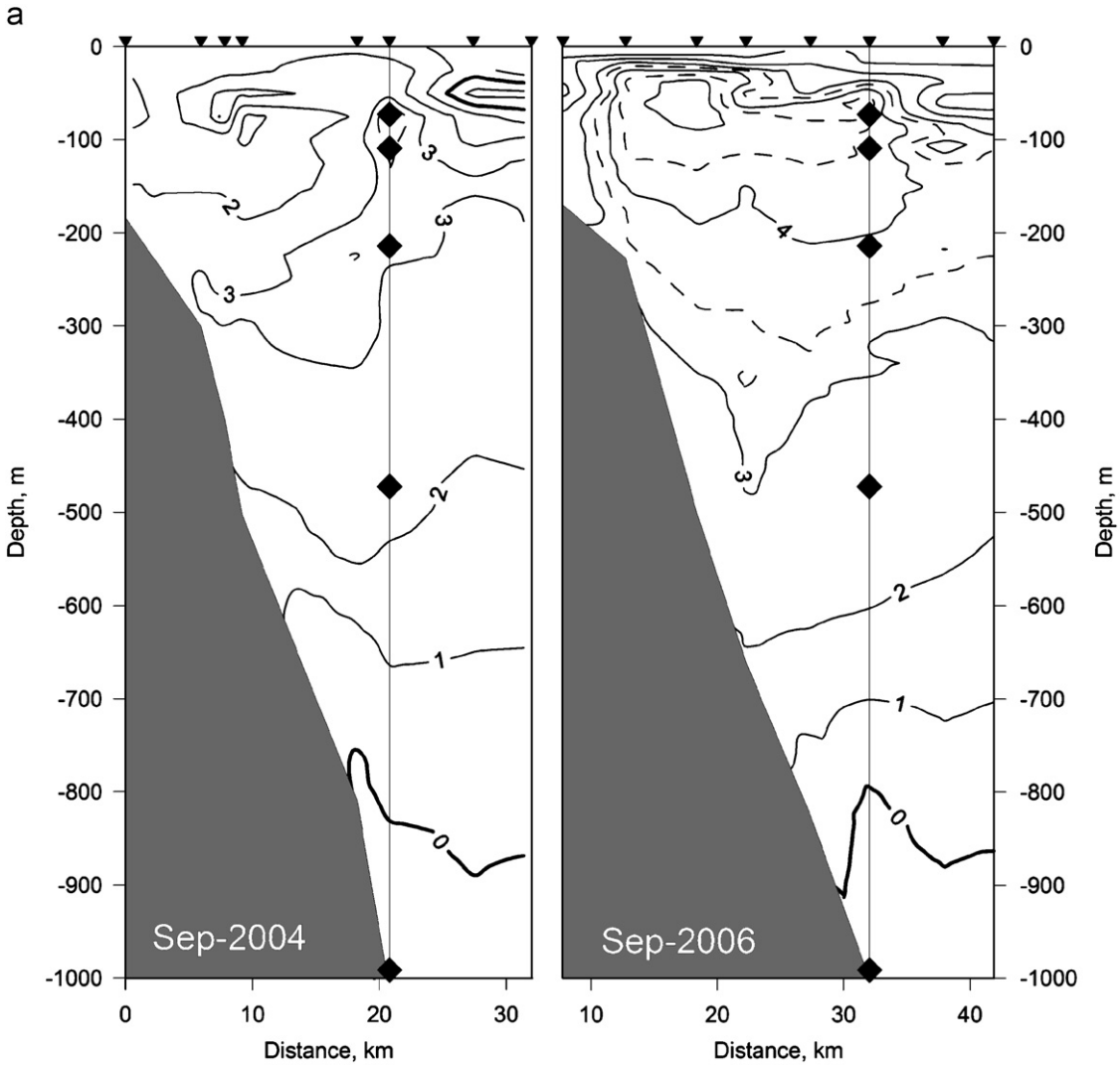

Fig. 2. Vertical sections of temperature (a) and salinity (b) across the continental slope at the mooring position in September 2004 and 2006. Black diamonds denote the location of moored instruments.

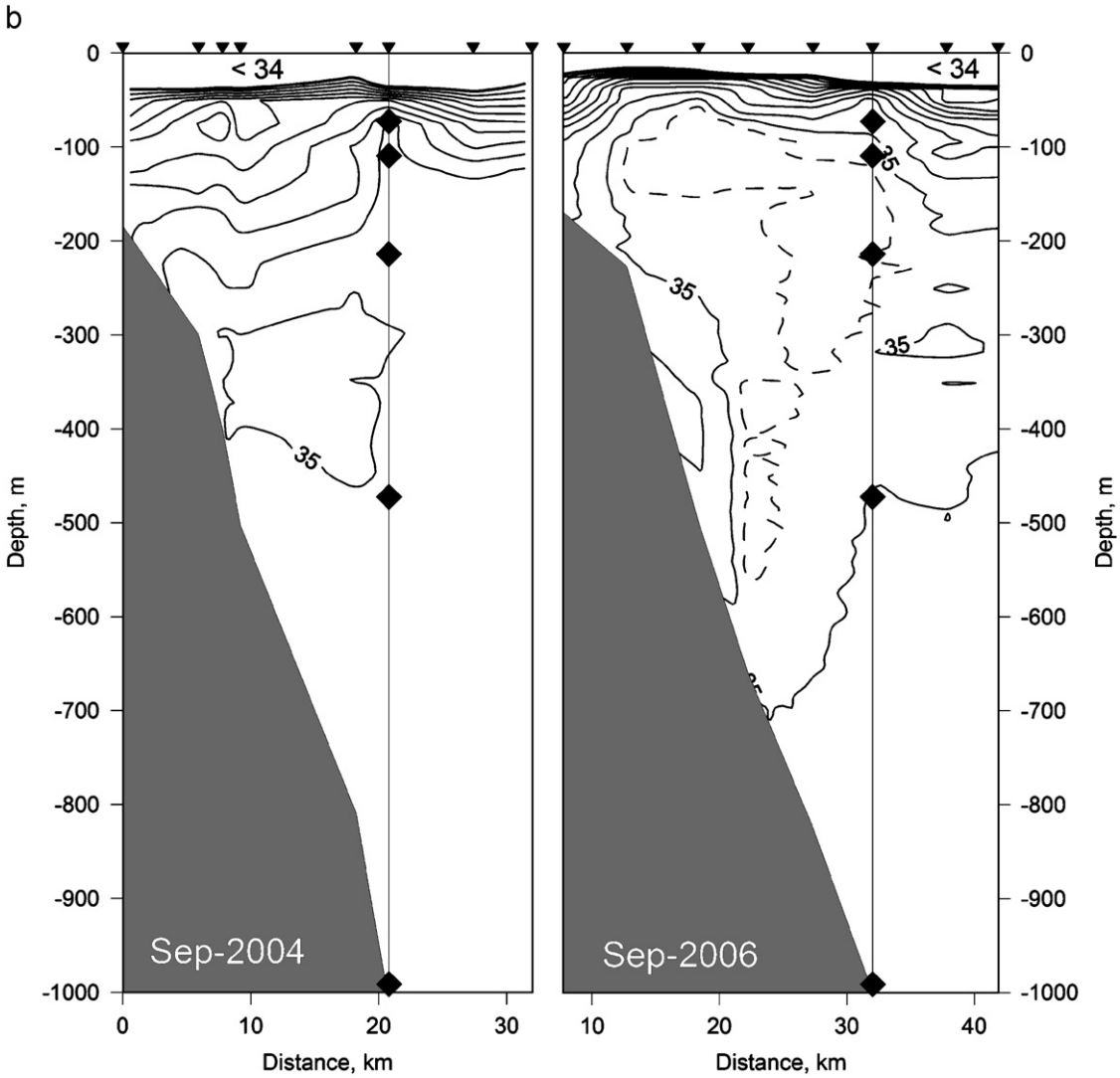

Fig. 2. (*Continued*)

data, CTD-based spatial means, and current measurements conducted earlier.

A typical scale of seasonal changes in temperature and salinity at the mooring position is illustrated by mean-summer and mean-winter climatologic profiles presented in Fig. 3. These profiles were calculated using the data from the Arctic Ocean Atlas (EWG, 1997, 1998). This Atlas contains a gridded dataset representing the average summer (July–September) and the average winter (February–April) temperature and salinity over the time interval 1950–1989. A substantial seasonal difference is observed in the upper 50 m layer. In winter, a cold and salty mixed layer replaces the relatively warm and fresh summer waters. Below the winter mixed layer the seasonal difference gradually decreases but is still traceable, reaching ~0.5 °C at 125 m. By 200 m the seasonal signal practically vanishes (although in the AW core, at 300 m, there is a hint that winter temperature is higher, by ~0.1 °C, than summer temperature).The seasonal salinity difference below the winter mixed layer is at the threshold of historical data accuracy.

Curves with circles in Fig. 3 show vertical distribution of temperature and salinity at the cross-slope section through the mooring position, averaged over two surveys (September 2004 and September 2006). These curves were calculated by horizontal averaging of the individual profiles over CTD sections shown in Fig. 2. During the mooring operation the entire AW layer was substantially warmer and saltier than would be expected from the 1950 to 1989 summer climatology. In the AW core at 200 m, the temperature deviation from climatology is as large as 1.7 °C and the salinity difference is about 0.1. Despite this apparent positive shift, characteristic features of the climatologic summer profile, including a subsurface temperature minimum at the base of the winter mixed layer, an intermediate temperature maximum in the AW

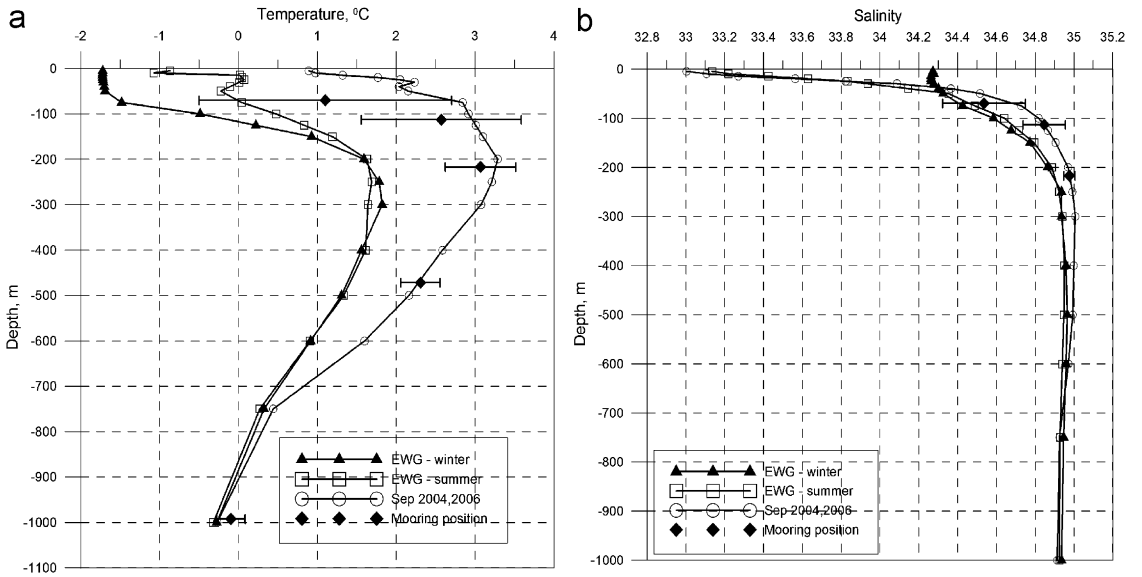

Fig. 3. Vertical distribution of temperature (a) and salinity (b) at the mooring position calculated using various averaging methods: (1) mean-summer (July–September) and mean-winter (February–April) climatologic profiles calculated by horizontal averaging of EWG (1997; 1998) gridded data within a 100 km circle around the mooring position are shown by black triangles and open squares correspondingly; (2) mean summer profiles calculated by horizontal averaging of individual T and S profiles over CTD sections and temporal averaging over September 2004 and 2006 surveys are shown by open red circles, and (3) 2 year means of mooring records are shown by diamonds bounded by standard deviation bars.

core, and strong freshening in the surface water layer remained unchanged in the horizontally averaged vertical profiles from September 2004 and 2006.

The vertical distribution of temperature and salinity calculated by averaging daily mooring data at sampled depths is shown by diamonds bounded by standard deviation bars in Fig. 3. There are several important features to be noted. Mooring-based mean vertical distributions have the same shape as seasonal climate profiles and CTD-based summer profiles, indicating that the moored instruments adequately resolve characteristic features of the vertical thermohaline structure. Averaged over the record, the temperature maximum of $3.07 \pm 0.45\,^{\circ}C$ is observed at 215 m. The temperature maximum from September 2004 to 2006 CTD data is $3.28\,^{\circ}C$, occurring at 200 m. Hence, we may expect that the instrument moored at 215 m depth was reasonably close to the AW warm core during most of its deployment. The scale of temperature and salinity temporal fluctuations quantified by standard deviation substantially exceed the summer–winter contrast derived from climatology. The temporal fluctuations of similar properties at three upper measured depths are highly correlated (see Table 1), indicating the coherent character of temporal variability in the upper part of the AW.

Two-month-long current observations carried out in the vicinity of Spitsbergen in July–September 1980 showed high (up to 30 cm/s) current velocity and persistent northeastward (i.e. along-slope) direction of flow (Aagaard, 1989). Our year-long measurements confirmed these findings (Fig. 4). However, our observations showed a different vertical distribution of current speed with a maximum of ~17 cm/s at 216 m (i.e. close to the AW warm core) whereas Aagaard (1989) found

Table 1
Temperature–temperature/salinity–salinity correlation coefficients at measured depths

Depth (m)	70	112	215	465
112	0.87/0.69			
215	0.52/0.30	0.68/0.54		
465	0.35/–	0.31/–	0.40/–	
992	−0.32/–	−0.41/–	−0.16/–	0.23/–

near-bottom intensification of the flow. The maximum current speed, measured by two upper instruments, exceeded 50 cm/s. Measurements taken during these extremely strong bursts of current were excluded from our analysis, since during these episodes the instruments were dragged to substantially greater depths. This truncation, however, exerted little effect on current statistics, because the high-speed episodes were of short duration (see Appendix A for details). Highly stable current direction at all measured depths indicates that at the mooring position AW flow is not subjected to intensive meandering and eddy formation. This finding is consistent with a stable location of the warm core relative to the bottom topography, which follows from the measured CTD sections and available historical observations (see Section 3.1).

3.3. Seasonal signal in temperature and salinity time series

We do not provide formal statistical estimates of the seasonal cycle for the current records, because those records are too short. Time series of temperature and salinity (T and S) are presented in Fig. 5. It is clear from

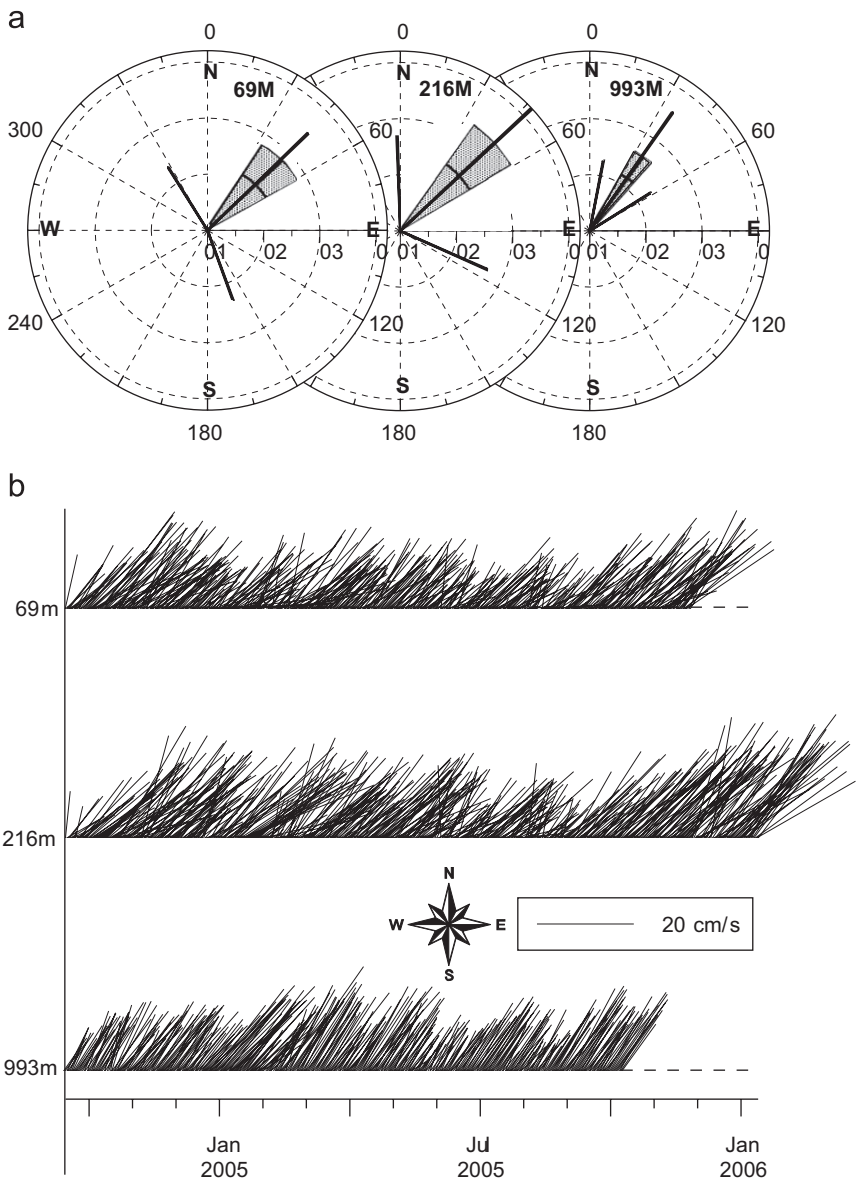

Fig. 4. (a) Statistical parameters of currents at the mooring position. Segments of circles, composed of radial and angular lines, show mean current vectors and one standard deviation of velocity and direction. Maximum current speed is shown by the radial line passing through the segment center. Total range of current direction variation is shown by radial lines encompassing the segment. (b) Daily current vectors at the mooring position.

visual inspection of temperature records that, despite relatively high levels of high-frequency fluctuations and trends, an annual cycle seems to prevail, at least at the upper three depth levels. The Fourier-based spectral analysis (Emery and Thomson, 2004) and Morlet wavelet transform of the T and S time series (Torrence and Compo, 1998) confirm this finding, displaying strong variability at the annual time scale (Table 2 and Figs. 6, 7). The annual mode of variability contributes up to 40–50% of the total T variance in the upper ocean (Fig. 6), and remains the major contributor to the T variations at intermediate depths (465 m) and near the bottom. Records of S are characterized by generally weaker seasonality. The largest contribution of the annual cycle to the total S variance is observed at 215 m (i.e. close to the AW core), the same depth at which the strongest T seasonal cycle is observed; however the annual cycle contribution to total S variance is ~20% smaller than the annual cycle contribution to the total T variance. Closer to the surface, the annual S cycle rapidly decreases. At the uppermost depth level (70 m) the annual S harmonic becomes less significant than the three sub-annual harmonics, contributing only 2% to the total variance. This difference of seasonality in the T and S records is confirmed by the wavelet transform (Fig. 7).

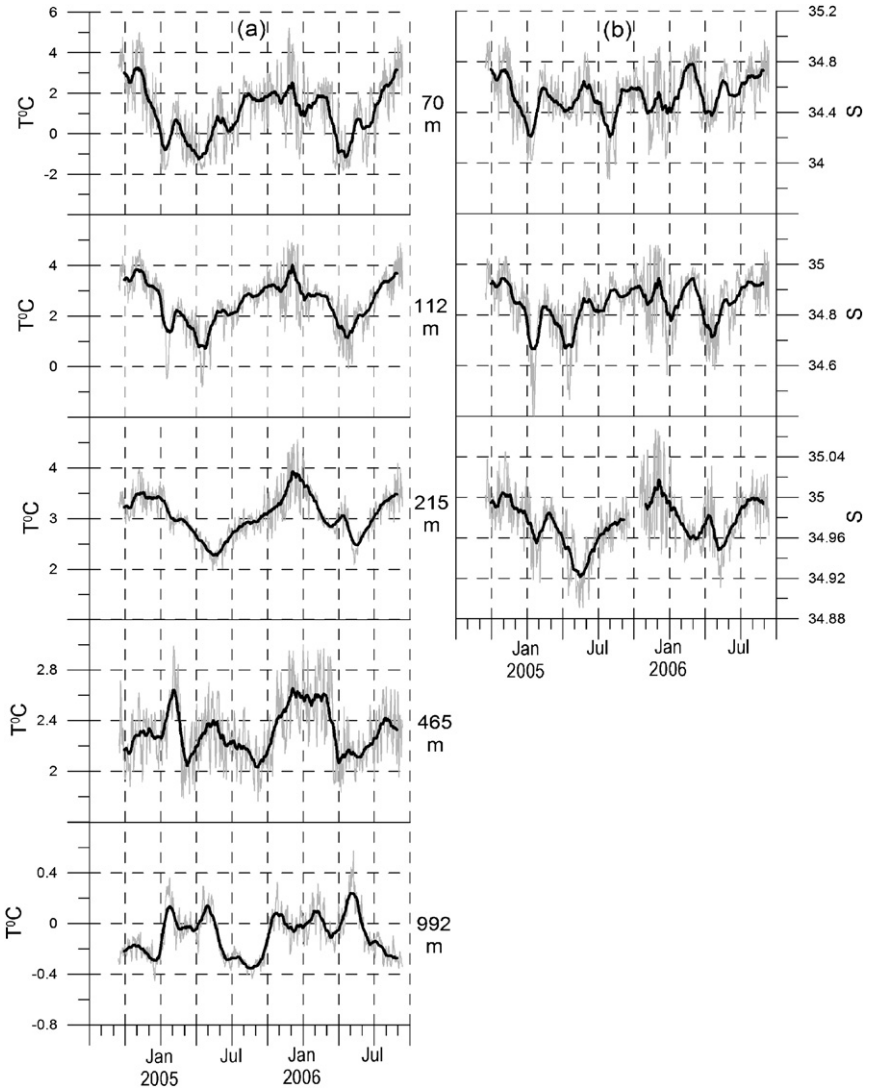

Fig. 5. Time series of temperature (a) and salinity (b) at the mooring position. Mean daily values are shown by thin lines; 1-month running averages are shown by thick lines.

Table 2
Relative contribution of the largest Fourier harmonic and the largest wavelet processes to the total variation of temperature and salinity

Parameter	Depth (m)	Largest Fourier harmonic			Largest wavelet process		
		Frequency (cycles/day)	Period (days)	Variation (%)	Frequency (cycles/day)	Period (days)	Variation (%)
Temperature	70	0.0027	365	41	0.0027	365	74
	112	0.0027	365	48	0.0027	365	77
	215	0.0027	365	53	0.0027	365	80
	465	0.0027	365	14	0.0033	303	38
	992	0.0027	365	33	0.0027	365	52
Salinity	70	0.0083	121	9	0.0085	118	27
	112	0.0027	365	19	0.0027	365	52
	215	0.0027	365	33	0.0027	365	64

At 215 m the S wavelet spectrum mirrors the T spectrum; S and T spectra are also similar at 112 m. At 70 m, the pattern of the S wavelet spectrum is very different than the patterns from 112 to 215 m, and also from the uppermost T wavelet spectrum; the maximum S wavelet spectrum energy is concentrated at higher frequencies

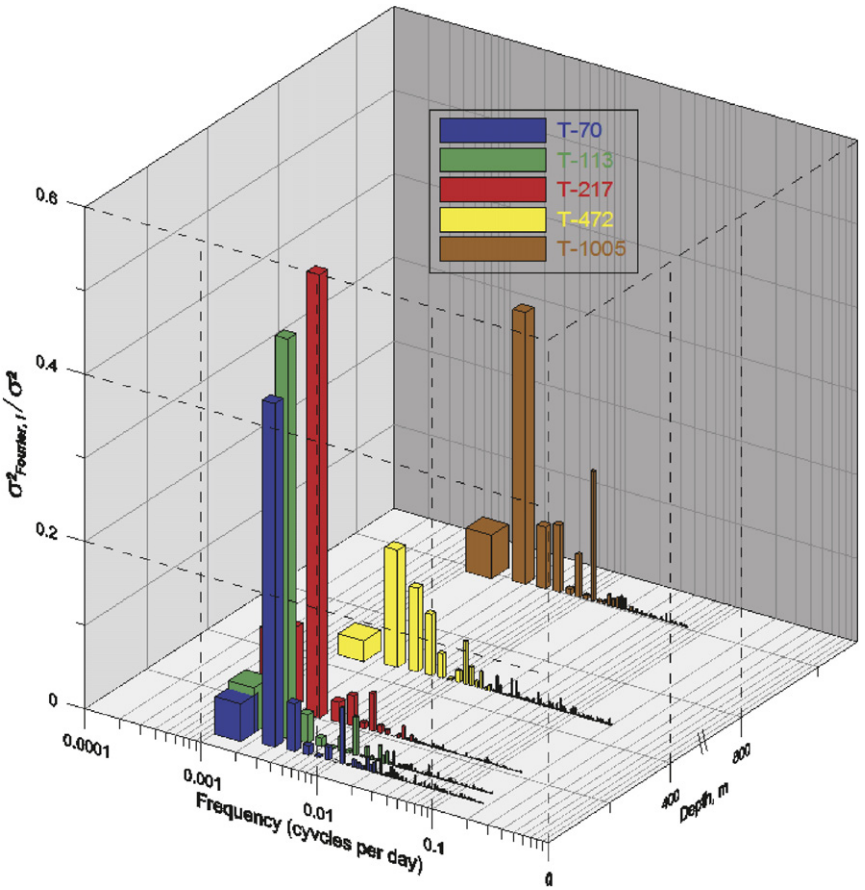

Fig. 6. Fourier line spectrum with power at discrete frequencies (cycles per day) for daily temperature time series.

corresponding to periods of 118, 165, and 236 days. This implies that the physics associated with S variation close to the surface differs from that of temperature variation.

For practical purposes it is important to know the amplitude (range) and the phase of the seasonal signal. The time series presented are too short for precise calculation of these parameters. Nevertheless, they allow us to carry out a rough estimation of range and phase for temperature time series at three upper levels, where the seasonal signal was the strongest. The zero-order estimation is provided by the Fourier annual harmonic, under the assumption that parameters of seasonal signal do not change from year to year (see Table 3). Using daily time series allows further rectification of this estimate. As follows from Fig. 5, low-pass filtering of daily data by applying a 1-month running averaging procedure significantly suppresses synoptic-scale oscillations, revealing the 'true' seasonal cycle. Since the optimal filter window width is not known, we experimented with varying window widths ranging from 3 to 121 days. The range of mean seasonal temperature variation as a function of window width is shown in Fig. 8a. Horizontal bars show the size of the difference in range between 2 years of measurements. The horizontal dashed line shows the range of the annual Fourier harmonic at corresponding depth. The range of seasonal temperature cycle at all three depths decreases consistently with the increasing width of the low-pass filter window, reaching the range of the annual Fourier harmonic for a window width of 90–100 days. The time interval between sequential minima and maxima (τ) for varying window widths is shown in Fig. 8b. At all three depths, after initial rapid change of τ at the stage of sequential filtering of synoptic and mesoscale noise there is an interval from 15 to 45 days where τ oscillates around some mean value. Further increase of the window width progressively changes τ until the boundaries start to affect it (at 90–100 days). Hence, we used the mid-point (31 days) of distinguished quasi-equilibrium interval as the width of the running average window to estimate the dates of minima/maxima and the range of seasonal signal from daily data. Results of these estimations are summarized in the corresponding columns in Table 3. The closest agreement in dates of minimum/maximum between Fourier annual harmonics and low-pass filtered daily temperature records is observed at 215 m. An annual temperature maximum in the upper part of the AW (above 215 m) is reached in mid-November. As derived from the low-pass filtered daily data, the seasonal cycle is asymmetrical (see Fig. 8b and Table 3). At the upper two levels the positive phase (temperature increase) takes about 7 months, while the negative phase is only 5 months in duration. At 215 m

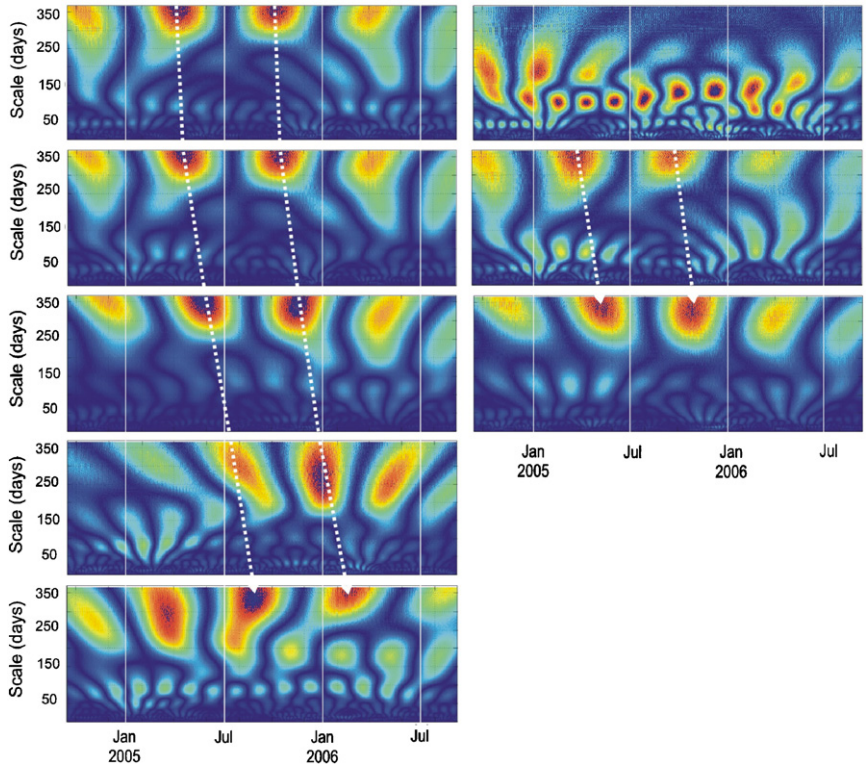

Fig. 7. The local wavelet power spectrum using Morlet wavelet transform of temperature at 70, 112, 215, 465, and 992 m (left column), and salinity at 70, 112, and 215 m (right column). Dotted white lines indicate phase shift of seasonal process at a scale of 365 days at different depths.

Table 3
Maxima/minima in temperature records

Depth (m)	Maximum, annual harmonic		Maximum, 31-day running average daily data		Minimum, annual harmonic		Minimum, 31-day running average daily data	
	Date	T (°C)	Date	T (°C)	Date	T (°C)	Date	T (°C)
70	October 6	2.46	November 18 ± 15	2.84 ± 0.42	April 6	−0.44	April 13 ± 10	−1.21 ± 0.04
112	October 16	3.56	November 17 ± 15	3.83 ± 0.02	April 16	1.57	April 23 ± 3	0.87 ± 0.18
215	November 19	3.53	November 25 ± 8	3.71 ± 0.19	May 19	2.61	May 21 ± 2	2.36 ± 0.10

Note: Daily data minima and maxima are taken as the average between two consecutive years.

warming and cooling intervals are nearly equal. These features are also distinguished by wavelet scalograms (see dotted white lines in Fig. 7). The range of seasonal temperature changes close to the AW core, at 215 m, is estimated to be between 0.92 and 1.35 °C. Maximum seasonal temperature variation (estimated to be between 2.90 and 4.05 °C) is observed at 70 m.

3.4. Definition of AW types

T–S diagrams at 70, 110, and 215 m indicate two clusters of daily T and S data (Fig. 9, right panels). Borders separating these clusters lie along the T–S linear regression lines calculated for the entire daily data sets at each depth. The use of different colors for points lying above and below regression lines reveals that the two clusters actually represent colder/fresher 'winter' (January–June) and warmer/saltier 'summer' (July–December) waters. This follows from the time series of temperature and salinity shown in Fig. 9—left panels. Statistical parameters of 'summer' and 'winter' waters are presented in Table 4. At all three depths the cooling/freshening ratio calculated using mean 'summer' and mean 'winter' properties is very high (see the last column in Table 4) indicating that observed seasonal change is predominantly thermally driven. The conclusion that the 'winter'–'summer' shift is defined mainly by the shift in temperature is also supported by the fact that the standard deviation of temperature within 'winter' and 'summer' clusters is smaller than the mean seasonal temperature difference (compare columns 4 and 5 in Table 4), while standard

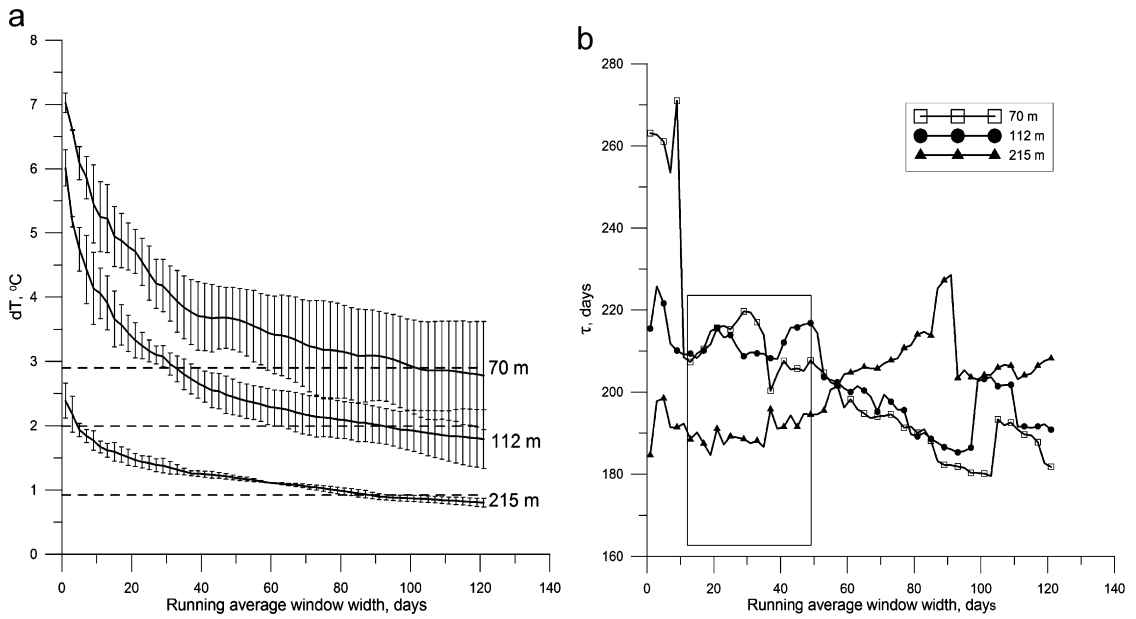

Fig. 8. (a) Mean range of seasonal temperature variation as a function of the running average window width and (b) time interval (τ) between sequential minimum and maximum for varying window width. The rectangle denotes the quasi-equilibrium time interval from 15 to 45 days (see the text).

deviation of 'winter'/'summer' salinity exceeds the 'summer'–'winter' salinity difference by an order of magnitude. The slope of the T–S regression line remains almost the same in both seasons (not shown), indicating an AW 'signature' at the position of the mooring throughout the entire year.

Seasonal alternation of 'summer' and 'winter' AW inflow changes the local heat content. We estimate that an annual water temperature change of 1.2 °C in the upper 215 m of the ocean (Table 4) results in a heat content fluctuation of $1.0 \times 10^9/\mathrm{m}^2$. This estimate is based on an assumption that ocean surface temperature is near the freezing point all year round, and assumes the specific heat of water at a constant pressure, $c_p = 4 \times 10^3\,\mathrm{J/kg/K}$, and water density, $\rho = 1.028 \times 10^3\,\mathrm{kg/m}^3$. The estimated value of seasonal heat content change is of the same order of magnitude as the mean AW heat content calculated for the western Nansen Basin from historical data (Dmitriev and Polyakov, 1995) suggesting that seasonal AW temperature change strongly affects the thermal regime at the mooring position.

4. Discussion and conclusions

The traditional concept of the AW layer in the Arctic Ocean does not admit significant seasonal variations of thermohaline properties within this layer. This concept may be considered to be perception by default, since the observational data required to check it are insufficient. On the other hand, existence of a strong seasonal cycle is well documented in Fram Strait AW at the doorstep to the Arctic Ocean interior (Schauer et al., 2004). In this study, we demonstrated that the strong seasonal cycle in the AW core 'survives' the 600 km transit from Fram Strait to 31°E, and 'diving' to an intermediate depth. This fact in itself may not be as important as what it implies for interpreting AW features observed in the Arctic Ocean. Instead of a steady decrease of AW temperature along the eastward-moving boundary flow, we may expect a periodic pattern with a wavelength defined by the advection length scale. According to this hypothesis, the multiple thermohaline anomalies reported in the AW layer in the 1990s on the basis of summer synoptic surveys (e.g. Quadfasel, 1991; Carmack et al., 1995; Swift et al., 1997) may not necessarily be caused only by interannual variations, but by the transformed seasonal signal as well.

According to our analysis, the range of seasonal signal close to the AW core at 31°E is estimated to be between 0.92 and 1.35 °C. The maximum measured increase of AW temperature during the 'Arctic Ocean warming' of the 1990s was about 1 °C over the climatic mean (Swift et al., 1997). The present AW warming, which was traced from the Nordic Seas through Fram Strait to the Laptev Sea, totals 0.8 °C (Polyakov et al., 2005; Dmitrenko et al., 2008). Taking these numbers into account, we may anticipate that the seasonal signal in the AW core temperature would be translated over long distances by the boundary current and be detected by long-term moored instruments. Amazingly, this is not the case. A year-long mooring observation at the eastern Laptev Sea slope provided no evidence of AW temperature modulation by an annual cycle (Woodgate et al., 2001), nor was this harmonic reported at the North Pole Environmental Observatory (NPEO) multi-year mooring (Morison et al., 2002). The only confirmation of the existence of seasonal variability in the AW core temperature has probably come from the multi-year Nansen and Amundsen Basin Observational System (NABOS) mooring in the southern Laptev Sea (Dmitrenko et al., 2006). Dmitrenko et al.

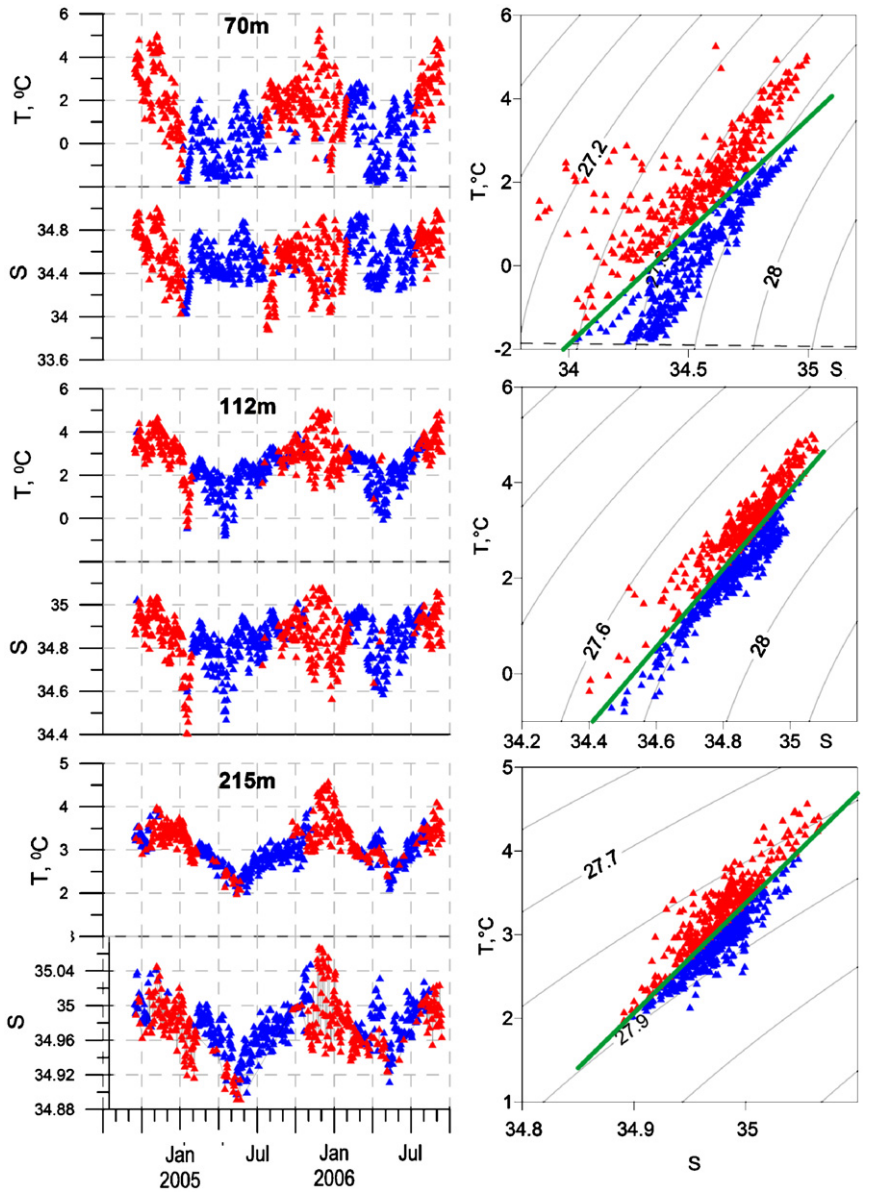

Fig. 9. Time series of daily temperature and salinity (left) versus corresponding T/S diagrams (right) at 70, 112, and 215 m. Green regression lines divide 'summer' and 'winter' waters. Dashed line shows the freezing temperature.

Table 4
Statistical parameters of 'winter' (W) and 'summer' (S) water at three upper depths

Depth (m)	Type of water	Number of days in 1 year	$\bar{T}$ (°C)	σ_T (°C)	$\bar{S}$	σ_S	$-\alpha(T_S-T_W)/\beta(S_S-S_W)$
70	W	183	0.12	1.28	34.52	0.19	5.3
	S	182	2.09	1.25	34.55	0.23	
112	W	199	2.10	0.86	34.83	0.10	4.2
	S	166	3.14	0.89	34.86	0.11	
215	W	203	2.88	0.34	34.975	0.03	15.5
	S	162	3.30	0.44	34.978	0.03	

Note: α—thermal expansion coefficient; β—salinity contraction coefficient.

(2006) attributed the observed annual variations to a cross-slope shift of the AW core caused by variation of local winds, but temperature change due to seasonal cycle was not ruled out.

What implications might the revealed division into 'summer' and 'winter' AW types have to the east of the mooring position, where warm water is permanently covered by a cold and freshened surface layer? According to our analysis, at the mooring position between 215 and 70 m, an annual temperature maximum, attributed to the 'summer' AW type, is reached around mid-November. This is the season when the surface water in the Nansen Basin is already at the freezing point and the ice rapidly grows, increasing upper mixed layer salinity and thickness. Sharpened temperature contrast and smoothed salinity contrast between the mixed layer and the underlying AW decrease vertical stability. Using mean temperature and mean salinity of 'winter' and 'summer' AW from Table 4 and climatologic parameters of the winter mixed layer (see Fig. 3), we can tentatively assess how important is this seasonal change. Mean winter temperature in the upper 50-m-thick mixed layer is $-1.71\,^{\circ}C$ and salinity is 34.28, which yields a potential density equal to 27.593. Potential density of the 'summer' water at 70 m is 27.604, while potential density of the 'winter' water is 27.712. This suggests that eastward propagation of warmer ('summer') AW during winter months provides favorable prerequisite conditions for deep convective mixing and subsequent release of heat from the upper part of the AW. Existing estimations point out that on its way between Fram Strait and Franz Joseph Land, the AW loses about half of its initial heat content (Treshnikov, 1977). Results of our study indicate that this strong release of heat might occur predominantly in winter when vertical stratification is weakened.

We summarize our findings related to seasonal variation in AW properties north of Spitsbergen as follows:

- Seasonal temperature variability is pronounced throughout the entire water column, contributing up to 50% of the total variance. Seasonal variation of salinity is strongest (40% of total variance) close to the AW core, but is substantially reduced towards the surface. No substantial seasonal variation was found in 1-year-long current records.
- The range of seasonal temperature changes close to the AW core, at 215 m, is estimated to be between 0.92 and $1.35\,^{\circ}C$. Maximum seasonal temperature variation (estimated to be between 2.90 and $4.05\,^{\circ}C$) is observed at 70 m. An annual temperature maximum in the upper part of the AW (above 215 m) is reached in mid-November when the ocean surface at the mooring position is normally covered by ice.
- Division into 'summer' (warmer and saltier) and 'winter' (colder and fresher) AW types is revealed in the upper part of the water column. The high cooling/freshening ratio calculated using mean 'summer' and mean 'winter' properties indicates that the observed seasonal change is predominantly thermally driven.
- The range of AW heat content variations due to alteration between 'summer' and 'winter' water types is of the same order of magnitude as the range of local mean AW heat content, suggesting an important role of seasonal changes in the intensity of the upward heat flux from AW.

By this paper, we would like to draw attention to the observation-based fact that the seasonal AW cycle 'survives' its transformation into Arctic intermediate water. Obvious temporal and spatial limitations of our data set do not allow us to precisely estimate seasonal cycle parameters. However, even the rough estimations presented here point out that seasonal fluctuations are sufficiently large that they should be taken into account in studies of temporal and spatial variability of the AW layer in the Arctic Ocean.

Acknowledgments

This research was supported by the ongoing NOAA and NSF funded NABOS Program, and the Frontier Research System for Global Change, Japan Agency for Marine-Earth Science and Technology (JAMSTEC).

Appendix A

Data checking and correction included the following sequential steps:

1. *Visual analysis of raw data scattering in* T/S *diagrams and parameter* vs. *time plots* resulted in the exclusion of 2519 salinity measurements made by SBE37 at 217 db. These data covered a continuous time span between September 19 and October 15, 2005. During this time interval unrealistically low salinity values were constantly measured. After this time interval salinity values returned to 'normal'.
2. *Pressure checking procedure*: All pressure readings were checked to verify that they fell inside the interval: (min. measured pressure, min. measured pressure+10 db). This interval is nearly the same as a ± 5 db range around the mean pressure level, which was measured by a corresponding device to be: 70, 113, 217, 472, and 1005 db for SBE37 measurements, and 69, 218, and 1006 db for RCM9 measurements. (All RCM9 pressure sensors did not work throughout the entire deployment, so only SBE37 pressure records were used.) Results of this procedure are presented in Table A1. On average, about 20% of readings were excluded from further analysis. Irrelevant data were occasionally generated when devices were carried far below the target depths of deployment, probably as a result of substantially increased current speed. For example, the correlation coefficient between the absolute value of horizontal speed and pressure at the 217 db level equals 0.81, increasing to 0.91 for current velocities exceeding 20 cm/s. Gaps in the data which appeared after this procedure were filled in by linear interpolation.
3. *Despiking procedure*: Measured values (X) which lay outside the interval $(\tilde{X}-2\sigma_X,\ \tilde{X}+2\sigma_X)$ were

Table A1
Data-checking statistics

Parameter	Pressure (db)	Total meas.	Kept after pressure correction		Kept after despiking	
			Number	%	Number	%
Temperature	70±5	70,009	53,235	76	52,974	76
	113±5	70,008	54,538	78	53,935	77
	217±5	70,009	53,750	77	53,264	76
	472±5	70,009	54,959	79	53,773	77
	1005±5	70,009	70,009	100	69,268	99
Salinity	70±5	70,009	53,235	76	51,954	74
	113±5	70,008	54,538	78	52,968	76
	217±5	70,009	51,231[a]	73	49,355	70
	472±5	70,009	54,959	79	54,689	78
	1005±5	70,009	70,009	100	69,842	99
Current velocity	69±5	10,575	8215	78	7388	70
	218±5	11,674	8912	76	8274	71
	1006±5	9413	9413	100	8755	93

[a] Including 2519 measurements that were removed after preliminary data checking.

replaced by $\tilde{X}$. $\tilde{X}$ is a 1-month running average; σ_X is the standard deviation. $\tilde{X}$ and σ_X were calculated after application of the pressure-checking procedure described above. About 2% of the measurements remaining after step 2 were removed by step 3.

4. *Checking* T and S *at the time of deployment/recovery against the CTD data*: The majority of CTD temperature and salinity measurements were in satisfactory agreement with mooring-based records, but there were two suspicious cases. Salinity records from SBE37s at 472 and 1005 db showed a strong negative salinity trend, which is not confirmed neither by temperature records taken by the same instrument, nor by accompanying CTD profiles, nor by salinity records from the other instruments. For this reason salinity records from the two lowest instruments were considered unreliable and excluded from further analysis.

After checking/correction procedures, all data were averaged over a 1-day interval to remove high-frequency tidal and inertial oscillations. Current direction was corrected by adding mean magnetic deviation (−16.82), calculated for the mid-time of deployment with the International Geomagnetic Reference Field Model 10 (IGRFM10) (http://www.ngdc.noaa.gov/IAGA/vmod).

References

Aagaard, K., 1989. A synthesis of Arctic Ocean circulation. Rapports P.-V. Réunion du Conseil International pour l'Exploration de la Mer 188, 11–22.

Carmack, E.C., Macdonald, R.W., Perkin, R.G., McLaughlin, F.A., Pearson, R.J., 1995. Evidence for warming of Atlantic Water in the Southern Canadian Basin of the Arctic Ocean: results from the Larsen-93 expedition. Geophysical Research Letters 22, 1061–1064.

Dmitrenko, I.A., Polyakov, I.V., Kirillov, S.A., Timokhov, L.A., Simmons, H.L., Ivanov, V.V., Walsh, D., 2006. Seasonal variability of Atlantic Water on the continental slope of the Laptev Sea during 2002–2004. Earth and Planetary Science Letters 244, 735–743.

Dmitrenko, I.A., Polyakov, I.V., Kirillov, S.A., Timokhov, L.A., Frolov, I.E., Sokolov, V.T., Simmons, H.L., Ivanov, V.V., Walsh, D., 2008. Towards a warmer Arctic Ocean: spreading of the early 21st century Atlantic Water warm anomaly along the Eurasian Basin margins. Journal of Geophysical Research.

Dmitriev, N.Eu., Polyakov, I.V., 1995. The Atlantic Water layer in the Arctic Basin. Geographical Description, Russian Meteorology and Hydrology 8, 19–23.

Emery, W.J., Thomson, R.E., 2004. Data Analysis Methods in Physical Oceanography. Elsevier, New York, p. 637.

Environmental Working Group (EWG), 1997, 1998. Joint US–Russian Atlas of the Arctic Ocean (CD-ROM), National Snow and Ice Data Centre, Boulder, Co., USA. WWW-page ⟨http://www.aari.nw.ru/index_en.html⟩.

Morison, J.H., Aagaard, K., Falkner, K.K., Hatakeyama, K., Moritz, R., Overland, J.E., Perovich, D., Shimada, K., Steele, M., Takizawa, T., Woodgate, R., 2002. North pole environmental observatory delivers early results. EOS Transactions 83.

Nikiforov, Ye.G., Shpaikher, A.O., 1980. Features of the formation of hydrological regime large-scale variations in the Arctic Ocean. Gydrometeoizdat, Leningrad, p. 269 (in Russian).

Polyakov, I.V., Proshutinsky, A.Yu., Johnson, M.A., 1999. The seasonal cycles in two regimes of Arctic climate. Journal of Geophysical Research 104 (C11), 25761–25788.

Polyakov, I.V., Beszczynska, A., Carmack, E.C., Dmitrenko, I.A., Fahrbach, E., Frolov, I.E., Gerdes, R., Hansen, E., Holfort, J., Ivanov, V.V., Johnson, M.A., Karcher, M., Kauker, F., Morison, J., Orvik, K.A., Schauer, U., Simmons, H.L., Skagseth, Ø., Sokolov, V.T., Steele, M., Timokhov, L.A., Walsh, D., Walsh, J.E., 2005. One more step towards a warmer Arctic. Geophysical Research Letters 32, L17605.

Quadfasel, D., 1991. Warming in the Arctic. Nature 350, 385.

Rudels, B., Anderson, L.G., Jones, E.P., 1996. Formation and evolution of the surface mixed layer and halocline of the Arctic Ocean. Journal of Geophysical Research 101 (C4), 8807–8821.

Rudels, B., Jones, E.P., Schauer, U., Eriksson, P., 2004. Atlantic sources of the Arctic Ocean surface and halocline waters. Polar Research 23 (2), 181–208.

Schauer, U., 1995. The release of brine-enriched shelf water from Storfjord into the Norwegian Sea. Journal of Geophysical Research 100 (C8), 16015–16028.

Schauer, U., Muench, R.D., Rudels, B., Timokhov, L., 1997. Impact of eastern Arctic shelf waters on the Nansen Basin intermediate layers. Journal of Geophysical Research 102 (C2), 3371–3382.

Schauer, U., Fahrbach, E., Osterhus, S., Rohardt, G., 2004. Arctic warming through the Fram strait: oceanic heat transport from 3 years of measurements. Journal of Geophysical Research 109, C06026.

Steele, M., Morison, J., Ermold, W., Rigor, I., Ortmeyer, M., Shimada, K., 2004. Circulation of summer Pacific halocline water in the Arctic Ocean. Journal of Geophysical Research 109, C02027.

Swift, J.H., Jones, E.P., Aagaard, K., Carmack, E.C., Hingston, M., MacDonald, R.W., McLaughlin, F.A., Perkin, R.G., 1997. Waters of the Makarov and Canada basins. Deep-Sea Research II 44 (8), 1503–1529.

Torrence, C., Compo, G.P., 1998. A practical guide to wavelet analysis. Bulletin of the American Meteorological Society 79, 61–78.

Treshnikov, A.F., 1977. Water masses of the Arctic basin. In: Dunbar, M.J. (Ed.), Polar Oceans. Arctic Institution of North America, pp. 17–31.

Woodgate, R.A., Aagaard, K., Muench, R.D., Gunn, J., Bjork, G., Rudels, B., Roach, A.T., Schauer, U., 2001. The Arctic Ocean boundary current along the Eurasian slope and the adjacent Lomonosov ridge: water mass properties, transports and transformations from moored instruments. Deep-Sea Research I 48, 1757–1792.